NANO LETTERS

pubs.acs.org/NanoLett

Letter

Laser Cooling of a Lattice Vibration in van der Waals Semiconductor

Jia-Min Lai, Yu-Jia Sun, Qing-Hai Tan, Ping-Heng Tan, and Jun Zhang*

Cite This: *Nano Lett.* 2022, 22, 7129−7135

Read Online

ACCESS | Metrics & More | Article Recommendations | Supporting Information

ABSTRACT: Laser cooling atoms and molecules to ultralow temperatures has produced plenty of opportunities in fundamental physics, precision metrology, and quantum science. Although theoretically proposed over 40 years, the laser cooling of certain lattice vibrations (i.e., phonon) remains a challenge owing to the complexity of solid structures. Here, we demonstrate Raman cooling of a longitudinal optical phonon in two-dimensional semiconductor WS_2 by red-detuning excitation at the sideband of the exciton (bound electron−hole pair). Strong coupling between the phonon and exciton and appreciable optomechanical coupling rates provide access to cooling high-frequency phonons that are robust against thermal decoherence even at room temperature. Our experiment opens possibilities of laser cooling and control of individual optical phonon and, eventually, possible cooling of matter in van der Waals semiconductor.

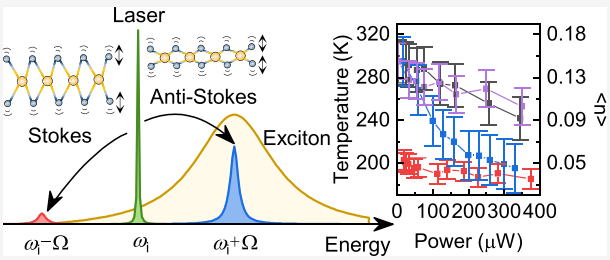

KEYWORDS: *Laser Cooling, Optical Phonon, van der Waals Semiconductor, WS_2*

In 1929, Peter Pringsheim first proposed that fluorescent gas can be cooled by optical irradiation.[1] After the laser was invented, dilute gases[2,3] where atomic interactions maintain the minimum can be cooled below 1 μK by laser. Ultracold atoms have fueled plenty of opportunities in precision metrology and quantum science. As interatomic interactions increase, atoms bond together and form molecules, where internal vibrational and rotational degrees of freedom also can be cooled to the quantum ground state by laser light.[4,5] In solids, atomic density reaches 10^{23} atoms/cm^3, and the thermal energy is primarily stored in the quanta of the atomic collective vibration, that is, phonons. In laser cooling of solids, the photoluminescence (PL) emits at higher energy than the incident laser, accompanied by phonon annihilation, that is, anti-Stokes photoluminescence (ASPL).[1] Over the past few decades, laser cooling of solids has been observed in many materials, such as rare-earth ion-doped crystals[6] and semiconductor nanostructures.[7−12]

As an extended work of ASPL, laser cooling of an individual phonon mode is important in solid-based quantum techniques. In solid cavity optomechanical systems, efficient narrow-band cooling of an individual phonon mode has been achieved through optical forces in geometry-engineered microstructures[13] and Brillouin scattering.[14,15] The laser cooling of local lattice vibrations in solids was first proposed by Dykman[16] and was further extended to the light-pressure cooling of lattice vibration by Javanainen.[17] However, it remains sparsely investigated experimentally for a long time. In 2016, Zhang et al. experimentally demonstrated the laser cooling of an individual optical phonon by strong exciton−phonon coupling (EPC) in ZnTe nanobelts.[18] Compared with cold atoms and molecules, laser cooling of a lattice phonon can provide fundamental insights for controlling internal vibrational degrees of freedom and exploring collective quantum effects in solids. Besides, excitons-mediated Raman cooling may be exploited to cool solid-state materials boding well for a new optical refrigeration form.[19−21] Therefore, it is very important to explore new materials for laser cooling of individual phonons.

Two-dimensional (2D) van der Waals (vdW) materials with atomic thickness show a robust exciton effect and strong EPC because of the confinement of dimension, reduced electrostatic shielding, and strong oscillator strength.[22,23] 2D materials, such as graphene[24] and transition-metal dichalcogenide (TMD)[25−27] semiconductors, have been used as oscillators in cavity optomechanical systems due to their low masses, small size, and high-quality factor. The characteristics of TMDs, such as valley polarization, strong spin−orbit coupling, and easy stacking to form heterostructures and moiré lattices,[28,29] provide plenty of cooling regulation degrees of freedom. In WS_2, the EPC is strong enough to observe many intriguing phenomena such as breakdown of the Raman selection rule,[23] Fano quantum interference,[30] and cross-dimensional EPC,[31] hinting at the possibility of laser cooling of lattice phonon. Motivated by the potential of atomic thin

Received: June 3, 2022
Revised: August 3, 2022
Published: August 22, 2022

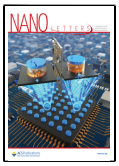

https://doi.org/10.1021/acs.nanolett.2c02240
Nano Lett. 2022, 22, 7129−7135

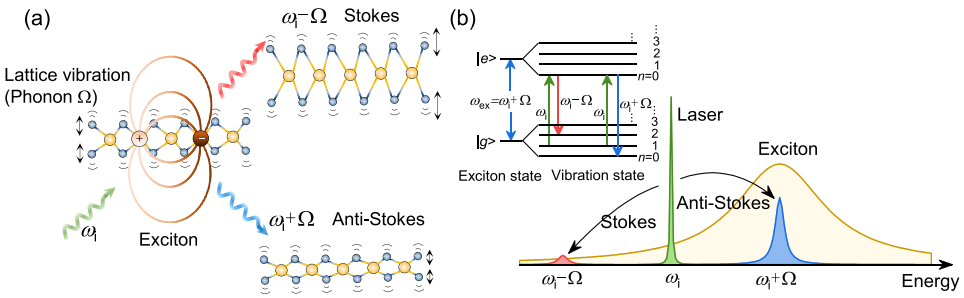

Figure 1. Principle of resolved-sideband Raman cooling of lattice vibration. (a) The schematic diagram of exciton−phonon interaction in monolayer WS_2 crystal. The ball-and-stick model represents the 2D lattice structure of WS_2 (W, yellow; S, blue). The balls with "+" "−" denote the electron−hole pair of an exciton. (b) The schematic spectrum diagram of sideband Raman cooling. (inset) The transition diagram of sideband Raman cooling. The green, red, and blue arrows denote the pump laser, Stokes scattering, and anti-Stokes scattering, respectively. $|n\rangle$ is the vibration levels. $|g\rangle$ and $|e\rangle$ are the ground state and excited state of the exciton, respectively.

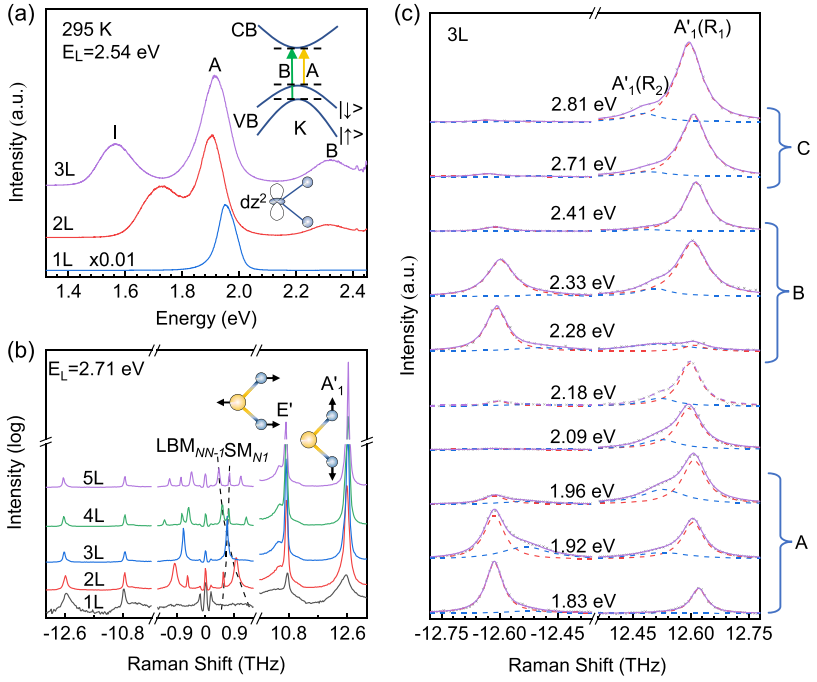

Figure 2. PL and Raman spectra of few-layer WS_2. (a) PL spectra of 1−3L WS_2 with 2.54 eV excitation at room temperature. I, A, and B represent the indirect exciton and A and B excitons, respectively. (inset) The schematics of A and B excitonic transition and electronic orbitals. (b) Raman spectra of 1−5L WS_2 excited at 2.71 eV. (inset) The vibration schematics of A'_1 and E′ phonon. (c) Raman spectra of A'_1-like Davydov components in 3L WS_2 excited by different laser energy. The red and blue dash lines and purple solid lines refer to the Lorentzian fitting results of $A'_1(R_1)$, $A'_1(R_2)$, and cumulative fitting curves, respectively. Excitons near the energy of the excitation laser are labeled on the right side.

semiconductors as versatile quantum materials, we demonstrate here the resolved-sideband Raman cooling of the longitudinal optical (LO) phonon (A'_1 mode of 12.6 THz) in 2D WS_2 by exciton resonance. By tuning the laser pump at the red sideband of the exciton, the A'_1 mode was attenuated to a colder state. Our study extends the possibility for laser cooling of internal phonon states in 2D vdW semiconductors.

Radiation pressure plays a core role in understanding the laser cooling of lattice phonons in classical pictures.[32] In solids, the radiation pressure results from the polarizability gradient of a laser field during light scattering, where the laser field exchanges energy with the lattice via scattering phonons. For Brillouin scattering, the acoustic phonons originate from the vibration of ions together with opposite charges, and the cooling or heating is dominated by the electrostrictive force.[14] For Raman scattering, optical phonon involves positive and negative ion vibrations against each other generating a macroscopic electronic field inside. In polar crystals, the light field interacts with the macroscopic polarization generated by LO phonon, called optoelastic force[18] $p_{oe} = \frac{1}{2}\varepsilon_0\left(\frac{\partial\chi}{\partial\Delta r}\right)E^2$. Here, ε_0, χ, E, and Δr denote the permittivity of free space, the electronic polarizability, the electric field of laser, and the relative displacement of oppositely charged atoms, respectively. Depending on the positive or negative work from the optoelastic force acting on lattice oscillations, the laser will enhance (heat) or attenuate (cool) the phonon oscillations.[18] See details in the Supporting Information.

The challenge of laser cooling is to enhance the phonon annihilation process (anti-Stokes scattering in Figure 1a) relatively over the phonon generation counterpart (Stokes scattering in Figure 1a). Resonant states created by electronic transitions at the microscopic scale[33] or photonic crystal engineered by the macroscopic structure of the materials[19]

https://doi.org/10.1021/acs.nanolett.2c02240
Nano Lett. 2022, 22, 7129−7135

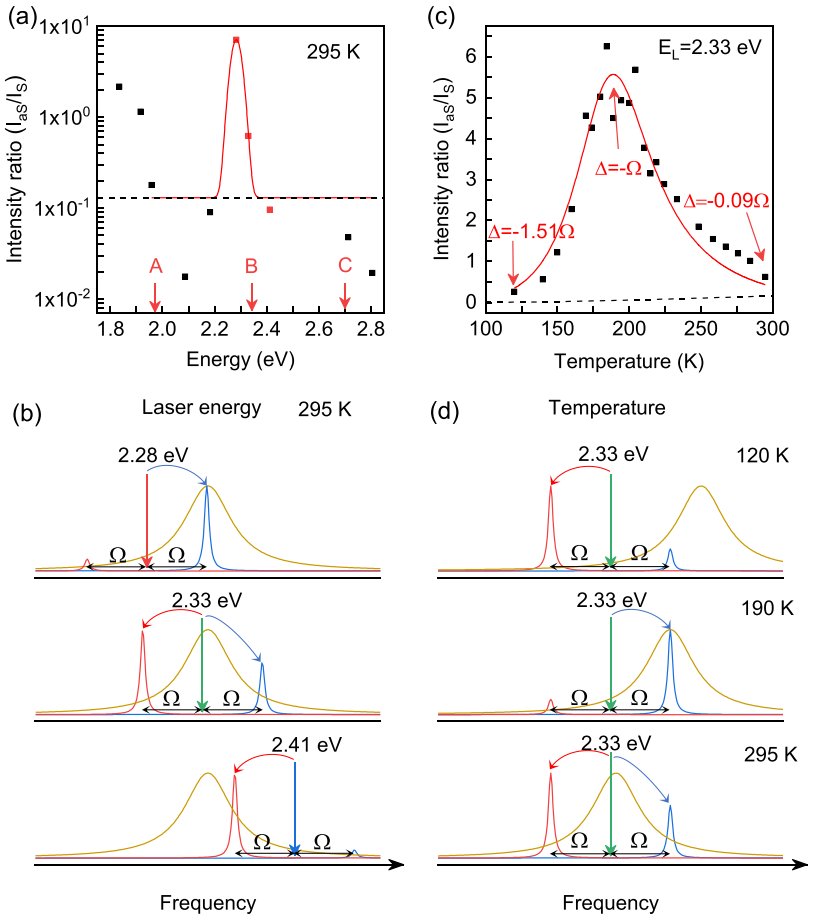

Figure 3. Breakdown of the thermal equilibrium between Stokes and anti-Stokes scattering. (a) I_{aS}/I_S of A′$_1$ phonon at different excitation laser energy. The energy of A, B, and C excitons is labeled at the energy axis. The dash line marks I_{aS}/I_S = 0.13 at thermal equilibrium. The red line is a Gaussian fitting result near B exciton. (b) The schematic spectra were excited by red-detuned (2.28 eV), zero-detuned (2.33 eV), and blue-detuned (2.41 eV) pump laser at room temperature. (c) The temperature-dependent I_{aS}/I_S of A′$_1$ phonon excited by 2.33 eV. The dash line marks I_{aS}/I_S under thermal equilibrium. The red line is the fitting result. (d) The schematic spectra excited by 2.33 eV at 120, 190, and 295 K.

provide means to achieve this nonequilibrium. Despite efforts to get close to the target,[8] it remains a major technical challenge due to the incredibly low Raman scattering efficiency until first success in ZnTe by using the naturally strong EPC.[18,20] Exciton, as the bound state of the electron−hole pair at the sub-band gap, can resonantly enhance the interaction between the incident laser field and the lattice phonon. As shown in Figure 1b, the incident laser ($\omega_i = \omega_{ex} - \Omega$) is red-detuned relative to the exciton (ω_{ex}) by exactly one phonon frequency (Ω); thus, the anti-Stokes scattering is resonant with the exciton and is significantly enhanced. It should be noted that "resolve" is the precondition of cooling to the quantum ground state of the individual phonon, which requires the exciton dissipation less than phonon energy ($\kappa_{ex} < \Omega$, where κ_{ex} is the damping rate of the exciton).[34,35] The corresponding energy-level diagram is shown in the inset. The incident laser pumps at the red phonon sideband of the exciton, and the lattice vibration state transition from $|n\rangle$ to $|n-1\rangle$ is resonantly enhanced, extracting one phonon energy from the lattice. Inversely, the Stokes process (from $|n\rangle$ to $|n+1\rangle$) with lattice absorption of phonons is nonresonant, and the transition rate is much less than anti-Stokes. The large nonequilibrium between anti-Stokes and Stokes will lead to a net annihilation of phonon. On the contrary, if we pump at the blue sideband of the exciton ($\omega_i = \omega_{ex} + \Omega$), Stokes scattering will be greatly enhanced, leading to phonon heating (even amplification by intense pumping). Therefore, it is crucial for the lattice phonon cooling in solids to find materials to achieve the reverse of the energy-flow direction in spontaneous Raman scattering. See the quantum theory and rate equation approach in the Supporting Information.

2D TMD semiconductors with a prominent exciton effect hint at the potential for phonon cooling due to strong EPC.[22,23] WS_2, as a typical 2D TMD semiconductor, has a hexagonal crystalline structure with each layer consisting of one W layer sandwiched between two S layers. As shown in the PL spectra of monolayer (1L), bilayer (2L), and trilayer (3L) WS_2 (Figure 2a), 1L WS_2 is a direct band gap semiconductor, while 2L, 3L to the bulk WS_2 are indirect band gap semiconductors ("I" labels the indirect transition). Three kinds of excitons can be observed in WS_2. A (~2.98 eV) and B (~2.35 eV) excitons are attributed to the transition from the spin−orbit split valence band and the lowest conduction at K (or K') point of the Brillouin zone,[36] as shown in the inset of Figure 2a. The C exciton (~2.70 eV) originates from the transition between the parallel bands around Γ point.

To identify the phonon modes and investigate the resonant enhancement of the anti-Stokes process, we performed the Raman spectra of few-layer WS_2. Figure 2b shows the Raman spectra of 1−5L WS_2 excited by 2.71 eV (close to the C

https://doi.org/10.1021/acs.nanolett.2c02240
Nano Lett. 2022, 22, 7129−7135

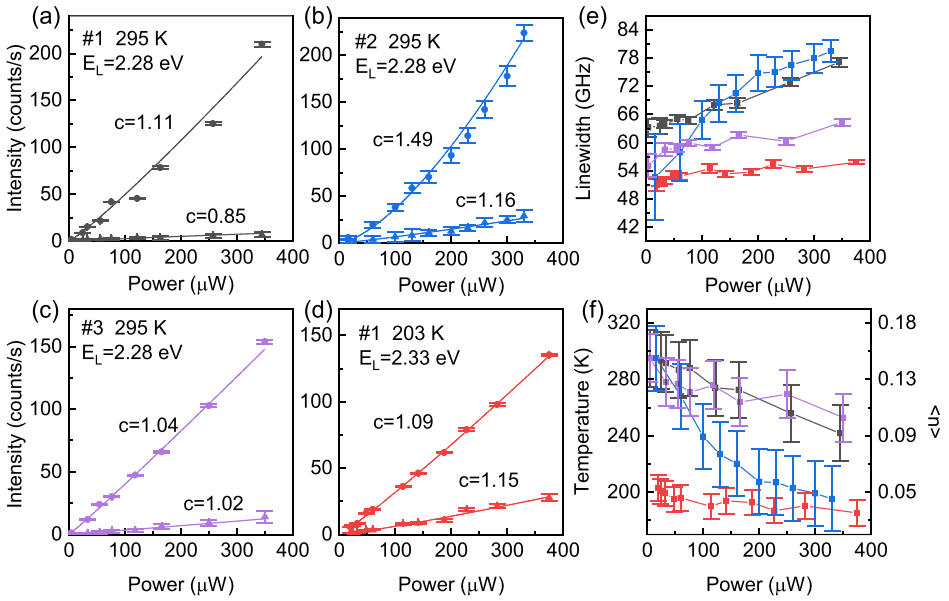

Figure 4. Power-dependent A'_1 mode intensity of Stokes (▲) and anti-Stokes (●) peaks of sample #1 (a), #2 (b), and #3 (c) at 295 K and #1 (d) at 203 K. Here, samples #1 and #2 are 3L WS_2, and sample #3 is an hBN-encapsulated 3L WS_2. The solid lines are fitted by the function of $I = aP^c$, where P is the power of excitation laser, and a and c are the fitting parameters. (e) The power-dependent linewidth of A'_1 phonon of different samples in (a−d). (f) The effective temperature and occupation number of A'_1 phonon of different samples in (a−d). The error bar was evaluated by the temperature fluctuation of Si signal and instrument response.

exciton). We can identify the first branch of interlayer shear modes (SM_{N1}) and $(N-1)$-th of breathing modes (LBM_{NN-1}) with typical frequency ($\Omega/2\pi$) from 556 to 753 GHz and from 956 to 421 GHz, respectively, whose layer number N dependency matches well with the theoretical results calculated by the linear chain model.[37] Two high-frequency modes are intralayer in-plane vibration E′ ($\Omega/2\pi \approx 10.7$ THz) and out-plane vibration A'_1 ($\Omega/2\pi \approx 12.6$ THz) phonon with Raman activity, respectively. We measured the Stokes and anti-Stokes Raman spectra of WS_2 at different excitation energy (Figure 2c) and found that the A'_1 mode shows relative intensity changes of anti-Stokes and Stokes signals, implying that the direction of the scattering energy flow can be tuned by controlling the detuning between laser and exciton. It should be noted that the relative intensity of anti-Stokes and Stokes signals in other modes (such as E′ in Supporting Information Figure S1) does not change so significantly. This can be understood by the symmetry of exciton orbitals and phonons.[38] A and B excitons reflect the d_{z^2} orbitals of the W atoms in the lowest WS_2 conduction band, and the exciton wave function is azimuthally symmetric, with the orbitals pointing along the z direction as shown in the inset of Figure 2a. The A'_1 mode involves out-of-plane vibration of S atoms, and therefore it can be more strongly coupled to A and B excitons than the in-plane mode E′. As for the C exciton, the electron has both W d_{z^2} and S p_x and p_y, with more S character near the hole. It can be inferred that the E′ mode phonon will show much stronger coupling with the C exciton,[30] though we did not observe a similar phenomenon of the E′ mode probably due to the inappropriate laser wavelength. Besides, the Davydov splitting of the A'_1-like mode was observed at resonant excitation labeled as $A'_1(R_1)$ and $A'_1(R_2)$.[30] The relative intensity of anti-Stokes and Stokes signal of $A'_1(R_2)$ (Figure S3) shows a slight deviation from $A'_1(R_1)$, which indicates that even a small vibration difference can cause large diversity in EPC. Since the intensity of $A'_1(R_2)$ is weak and greatly affected by fitting, we mainly study the $A'_1(R_1)$ mode (abbreviated as A'_1 hereinafter).

As discussed above, by changing the detuned frequency of laser and exciton ($\Delta = \omega_i - \omega_{ex}$), the Stokes and anti-Stokes sideband become nonequilibrium, implying that the exciton resonant situation induces the energy extracted from or added to the lattice vibration; that is, the A'_1 phonon can be cooled or heated. Apparently, the resonance situation can be regulated by selecting the laser energy or adjusting the exciton energy. We extract the intensity ratio of anti-Stokes and Stokes (I_{aS}/I_S) of A'_1 mode in Figure 3a from Figure 2c. The anti-Stokes scattering and Stokes scattering are related to the phonon annihilation and creation process, and thus their intensities are proportional to phonon population n and $(n+1)$, respectively. Under the thermal equilibrium, $I_{aS}/I_S = \left(\frac{\omega_i+\Omega}{\omega_i-\Omega}\right)^4 \frac{\bar{n}}{\bar{n}+1}$, where the phonon occupation number $\bar{n} = \left[\exp\left(\frac{\hbar\Omega}{k_BT}\right) - 1\right]^{-1}$ satisfies the Bose−Einstein distribution, and $\frac{\omega_i+\Omega}{\omega_i-\Omega}$ is close to the unit because the phonon frequency is much less than the incident laser frequency. For the A'_1 phonon, at bath temperature (295 K), $I_{aS}/I_S = 0.13$. Near the A exciton and B exciton, the I_{aS}/I_S varies from 7.10 (>0.13) to 0.018 (<0.13) when the excitation laser frequency is detuned from red to blue. It suggests that, compared with thermal equilibrium, under red (or blue) detuning excitation, the scattering process is dominant by phonon annihilation (or creation). By fitting the profile of I_{aS}/I_S around the B exciton, we can approximately evaluate the linewidth of B exciton is 41 meV ($\kappa_{ex}/2\pi \approx 9.91$ THz), which is less than the energy of A'_1 phonon, satisfying the requirement of resolved-sideband cooling. As shown in Figure 3b, when the laser energy is at the red-detuned sideband (2.28 eV), $\Delta = \omega_i - \omega_{ex} = -1.02\Omega$, and the incident photon is scattered to the exciton resonance with the A'_1 phonon transition to the lower vibration state. According to the

https://doi.org/10.1021/acs.nanolett.2c02240
Nano Lett. 2022, 22, 7129−7135

optomechanics theory,[18,34,35] the red-detuned laser will add extra damping (Γ_{opt}) to the oscillator and decrease the occupation number of the phonon, leading to phonon cooling. Inversely, if the laser pumps at the blue-detuned (2.41 eV) sideband of B exciton, $\Delta = \omega_i - \omega_{ex} = 1.45\Omega$, the damping decreases, and the occupation number of the phonon increases, leading to phonon heating or amplification. Particularly, if the energy of the pump laser is very close to that of the B exciton ($\Delta = -0.09\Omega$), I_{aS}/I_S tends to the value of thermal equilibrium, providing potential for quantum nondemolition detection of the optical amplitude quadrature.

We also measured the temperature-dependent Raman spectra excited by the 2.33 eV laser (Figure S4) and extracted the intensity ratio in Figure 3c. The temperature-dependent experiments were measured at red-detuned sideband; thus, I_{aS}/I_S values are larger than the value under thermal equilibrium. The maximum is at 190 K corresponding to $\Delta = \omega_i - \omega_{ex} = -\Omega$. Considering the resonance with exciton level, I_{aS}/I_S has a Lorentzian profile, and it can be expressed as

$$I_{aS}/I_S \propto \frac{\overline{n}}{\overline{n}+1}\frac{(\Delta-\Omega)^2+(\kappa_{ex}/2)^2}{(\Delta+\Omega)^2+(\kappa_{ex}/2)^2}$$

Since the temperature will affect the exciton energy and linewidth, we introduce the Varshni equation[39] $E(T) = E(0) - \alpha T^2/(T+\beta)$ and linear equation to simply describe the peak position and linewidth of the exciton, respectively. Then, we obtain

$$I_{aS}/I_S \propto \exp\left(\frac{\hbar\Omega}{k_B T}\right)\frac{(E_i - E(0) + \alpha T^2/(T+\beta) - \hbar\Omega)^2 + (aT/2)^2}{(E_i - E(0) + \alpha T^2/(T+\beta) + \hbar\Omega)^2 + (aT/2)^2}$$

where β is the Debye temperature of WS_2, $E(0)$ is the exciton energy at 0 K, E_i is the energy of the incident laser, and α and a reflect the temperature coefficient of the exciton shift and linewidth, respectively. To fit the temperature-dependent I_{aS}/I_S, we obtained the Debye temperature of trilayer WS_2 is 205 K, which is consistent with the previous report.[40] The fitting linewidth of the exciton at 295 K is 44.25 meV ($\kappa_{ex}/2\pi \approx 10.68$ THz) close to the result acquired by the excited energy-dependent I_{aS}/I_S, improving the confidence of resolved sideband Raman cooling. Figure 3d shows the schematics pumped at three temperatures corresponding to the red detuning at -1.51Ω, $-\Omega$, and -0.09Ω, which is perfectly consistent with the theory of optomechanics.[34,35]

To evaluate the cooling results, we measured the power-dependent Stokes and anti-Stokes scattering intensity of the A'_1 mode of three samples #1, #2, and #3 at 295 K and #1 at 203 K as shown in Figure 4a–d. We use a very low-power (<400 μW) laser, so the sample can easily exchange heat with the surroundings including the substrate to reach thermal equilibrium. The effect of laser heating and instrument response are excluded by the Raman signal of Si substrate (Figure S5). In addition, Figure 3c shows that, at the red sideband of the exciton, even a slight temperature deviation from the exciton resonance point can significantly reduce I_{aS}/I_S. In the power-dependent results, the I_{aS}/I_S of the A'_1 mode does not decrease, providing assertive evidence to exclude laser heating. The anti-Stokes intensity for sample #2 shows nonlinear dependence on laser power, suggesting that it might involve a nonlinear mechanism with the excitation power increase. As discussed in our previous reports,[18] there are two thermometry methods to determine the phonon occupation number and effective temperature. The Raman intensity method requires extremely well-calibrated amplitude measurements, which potentially are susceptible to drifts during experiments. Another clearer confirmation of temperature reduction can be obtained by inferring the light-induced damping of the phonon from the phonon spectral line shape.[13,41] Figure 4e shows the power-dependent linewidth of the A'_1 mode. The effective temperature of the cooled phonon can be evaluated by the linewidth ratio:[13,34,41] $T_{final} = T_{initial}\frac{\Gamma_{initial}}{\Gamma_{final}}$. Here, the final linewidth $\Gamma_{final} = \Gamma_0 + \Gamma_{opt}$ is the sum of intrinsic damping of phonon Γ_0 and the extra damping induced by driving laser Γ_{opt}, and the initial linewidth $\Gamma_{initial}$ is measured with enough low laser power to keep the thermal equilibrium between target phonon and sample bath. Red-detuned laser adds external damping ($\Gamma_{opt} > 0$) to the phonon oscillation, and the work acted on the lattice oscillator is negative; thus, the phonon was driven to a cooler state. In this way, we obtained the power dependency of the phonon temperature and further the corresponding occupancy number $\overline{n}$ through the Bose–Einstein distribution (Figure 4f). For samples #1 and #3, the phonon can be cooled to about 240 and 250 K from the bath temperature (295 K) with $\overline{n}$ from 0.15 to 0.088 and 0.099, and the corresponding ground-state occupation possibility ($P_{\overline{n}=0} = \frac{1}{1+\overline{n}}$) is from 87.0% to 91.9% and 91.0%, respectively. Notably, sample #2 shows a significantly greater temperature decrease (from 295 to 195 K with $\overline{n}$ to 0.048 and the ground-state occupation possibility to 95.4%) than others, suggesting the nonlinear cooling mechanism can lead to higher cooling efficiency, while for sample #1 excited by 2.33 eV at 203 K, the A'_1 phonon was cooled to about 185 K from the bath temperature (203 K) with $\overline{n}$ from 0.054 to 0.040 and the ground-state occupation possibility from 94.9% to 96.2%. It suggests that the cooling effects of the laser diminish as the temperature decreases. The existence of the cooling limitation is attributed to three factors:[21,34] (1) The thermal nonequilibrium between the cooled phonon mode and the entire phonon bath (or heat sink) will lead to the thermal energy "leak" back in, which intensifies as the phonon temperature is reduced; (2) The parasitic laser absorption (e.g., two-photon absorption and nonradiation recombination) effect causes heating of the whole sample; (3) The laser heating also influences the energy and linewidth of the exciton altering the detuning situation. Elimination of these parasitic sample heating effects might reach a deeper cooling effect.

The coupling factor g is the key parameter to evaluate the coupling strength of the optomechanics system. To estimate the coupling factor between the phonon and exciton, we use an analogy with the damping rate and frequency in optomechanics. The extra damping rate of the phonon is given by[13,34,41] $\Gamma_{opt} = g^2\left(\frac{\kappa_{ex}}{\kappa_{ex}^2/4+(\Delta+\Omega)^2} - \frac{\kappa_{ex}}{\kappa_{ex}^2/4+(\Delta-\Omega)^2}\right)$, where $\Gamma_{opt} = \Gamma_{final} - \Gamma_0$. The frequency shift of the phonon induced by the light field can be written as[34] $\delta\Omega = g^2\left(\frac{\Delta+\Omega}{\kappa_{ex}^2/4+(\Delta+\Omega)^2} + \frac{\Delta-\Omega}{\kappa_{ex}^2/4+(\Delta-\Omega)^2}\right)$. Substitute the relevant parameters of sample #1, and we obtain g = 392 GHz and Γ_0 = 21.8 GHz of the A'_1 phonon (see the calculation for other samples in

https://doi.org/10.1021/acs.nanolett.2c02240
Nano Lett. 2022, 22, 7129–7135

Table S1). Such strong coupling between phonon and exciton leads to the effective cooling of the A'_1 phonon.

In conclusion, we demonstrate the Raman cooling of an optical phonon in a vdW semiconductor. Compared with acoustic phonons, high-frequency optical phonons can be initialized in the quantum ground state at a higher bath temperature. Furthermore, exciton-mediated Raman cooling may provide a new refrigeration form to cool solid-state materials.[19−21] Although the Raman cooling efficiency can reach 5%−10% per scattered photon (calculated via the energy ratio of phonon to photon), the small scattering probability leads to very low single-pass net cooling efficiency ($\sim 10^{-7}$ cm^{-1}).[19] Here, the exciton-enhanced anti-Stokes Raman mechanism involves a real transition; thus, the Raman scattering probability can be boosted up several orders of magnitude,[21] and the efficiency increases as discussed in the Supporting Information. In view of the net cooling of solids, the phonon anharmonicity related to the heat transfer between cold phonons and other hot phonons needs to be considered. It can be speculated that all of the phonon modes would reach thermal equilibrium only if the laser excites for enough time. Furthermore, improving efficiency is also in favor of net cooling, such as strategically placed anti-Stokes resonances through photonic density of state, exploring nonlinear mechanisms, etc.

EXPERIMENT METHODS

The samples were prepared from bulk WS_2 crystals onto SiO_2/Si substrates using the micromechanical exfoliation technique. Raman measurements were undertaken in backscattering geometry with a Jobin-Yvon HR800 system equipped with a liquid-nitrogen-cooled charge-coupled detector (CCD). The PL spectra and Raman spectra were detected with 600 lines/mm and 1800 line/mm grating, respectively. The room-temperature Raman spectra were collected with a 100× objective lens (numerical aperture (NA) = 0.9). The temperature-dependent Raman spectra were collected with a 50× objective lens (NA = 0.5) with a helium-cooled cryogenic station (Montana Instruments) at a vacuum of 10^{-1} mbar. The excitation laser line of 2.81 eV is from a He−Cd laser; the laser lines from of 2.71, 2.54, and 2.41 eV are from an Ar^+ laser; the laser lines of 2.33, 2.18, 1.92, and 1.83 eV are from a Kr^+ laser; the laser lines of 2.28, 2.09, and 1.96 eV are from a He−Ne laser. The ultralow-frequency Raman spectra were obtained down to ±5 cm^{-1} by combining three volume Bragg grating filters into the Raman system to efficiently suppress the Rayleigh signal.

ASSOCIATED CONTENT

Supporting Information

The Supporting Information is available free of charge at https://pubs.acs.org/doi/10.1021/acs.nanolett.2c02240.

The classical theory of radiation pressure. Quantum theory of exciton−phonon coupling with a driven optical field. Rate equation approach of radiation-pressure cooling. The frequency shift and the extra damping rate during laser cooling. Raman spectra of E′ mode in 3L WS_2 excited by different laser energy (Figure S1). Layer-dependent Raman spectra of A'_1 mode (Figure S2). The intensity ratio I_{aS}/I_S of A'_1 phonon at different excitation laser energy (Figure S3). Temperature-dependent Raman spectra of A'_1 mode and Si (Figure S4). The power dependence of intensity ratio I_{aS}/I_S of Si (Figure S5). The calculated coupling factor g and intrinsic linewidth Γ_0 (Table S1) (PDF)

AUTHOR INFORMATION

Corresponding Author

Jun Zhang − *State Key Laboratory of Superlattices and Microstructures, Institute of Semiconductors, Chinese Academy of Sciences, Beijing 100083, China; Center of Materials Science and Optoelectronics Engineering and CAS Center of Excellence in Topological Quantum Computation, University of Chinese Academy of Sciences, Beijing 100049, China;* orcid.org/0000-0002-9831-6796; Email: zhangjwill@semi.ac.cn

Authors

Jia-Min Lai − *State Key Laboratory of Superlattices and Microstructures, Institute of Semiconductors, Chinese Academy of Sciences, Beijing 100083, China; Center of Materials Science and Optoelectronics Engineering, University of Chinese Academy of Sciences, Beijing 100049, China*

Yu-Jia Sun − *State Key Laboratory of Superlattices and Microstructures, Institute of Semiconductors, Chinese Academy of Sciences, Beijing 100083, China; Center of Materials Science and Optoelectronics Engineering, University of Chinese Academy of Sciences, Beijing 100049, China*

Qing-Hai Tan − *State Key Laboratory of Superlattices and Microstructures, Institute of Semiconductors, Chinese Academy of Sciences, Beijing 100083, China;* orcid.org/0000-0003-4808-4795

Ping-Heng Tan − *State Key Laboratory of Superlattices and Microstructures, Institute of Semiconductors, Chinese Academy of Sciences, Beijing 100083, China; Center of Materials Science and Optoelectronics Engineering, University of Chinese Academy of Sciences, Beijing 100049, China;* orcid.org/0000-0001-6575-1516

Complete contact information is available at: https://pubs.acs.org/10.1021/acs.nanolett.2c02240

Author Contributions

J.Z. conceived the project. J.L., Y.S., and Q.T. performed experiments. J.L. and J.Z. analyzed the data and wrote the paper. All the authors discussed the results and revised the paper.

Notes

The authors declare no competing financial interest.

ACKNOWLEDGMENTS

J.Z. acknowledges the National Key Research and Development Program of China (2017YFA0303401), CAS Interdisciplinary Innovation Team, National Natural Science Foundation of China (12074371), Strategic Priority Research Program of Chinese Academy of Sciences (XDB28000000).

REFERENCES

(1) Pringsheim, P. Zwei Bemerkungen über den Unterschied von Lumineszenz- und Temperaturstrahlung. *Zeitschrift für Physik* **1929**, *57* (11−12), 739−746.

(2) Hänsch, T. W.; Schawlow, A. L. Cooling of gases by laser radiation. *Opt. Commun.* **1975**, *13* (1), 68−69.

(3) Pool, R. Laser cooling hits new low. *Science* **1990**, *248* (4959), 1077.

(4) Mitra, D.; Vilas Nathaniel, B.; Hallas, C.; Anderegg, L.; Augenbraun Benjamin, L.; Baum, L.; Miller, C.; Raval, S.; Doyle John, M. Direct laser cooling of a symmetric top molecule. *Science* **2020**, *369* (6509), 1366−1369.
(5) Bohn, J. L.; Rey, A. M.; Ye, J. Cold molecules: Progress in quantum engineering of chemistry and quantum matter. *Science* **2017**, *357* (6355), 1002−1010.
(6) Seletskiy, D. V.; Epstein, R.; Sheik-Bahae, M. Laser cooling in solids: advances and prospects. *Rep. Prog. Phys.* **2016**, *79* (9), 096401.
(7) Li, D.; Zhang, J.; Wang, X.; Huang, B.; Xiong, Q. Solid-State Semiconductor Optical Cryocooler Based on CdS Nanobelts. *Nano Lett.* **2014**, *14* (8), 4724−4728.
(8) Zhang, J.; Li, D.; Chen, R.; Xiong, Q. Laser cooling of a semiconductor by 40 K. *Nature* **2013**, *493* (7433), 504−508.
(9) Ha, S.-T.; Shen, C.; Zhang, J.; Xiong, Q. Laser cooling of organic-inorganic lead halide perovskites. *Nat. Photonics* **2016**, *10* (2), 115−121.
(10) Ye, Z.; Lin, X.; Wang, N.; Zhou, J.; Zhu, M.; Qin, H.; Peng, X. Phonon-assisted up-conversion photoluminescence of quantum dots. *Nat. Commun.* **2021**, *12* (1), 4283.
(11) Roman, B. J.; Villegas, N. M.; Lytle, K.; Sheldon, M. Optically Cooling Cesium Lead Tribromide Nanocrystals. *Nano Lett.* **2020**, *20* (12), 8874−8879.
(12) Xu, W.; Zhao, Y.; Shen, C.; Zhang, J.; Xiong, Q. Phonon-assisted Upconversion Photoluminescence in Monolayer $MoSe_2$ and WSe_2. *Acta Chim. Sin.* **2015**, *73* (9), 959−964.
(13) Arcizet, O.; Cohadon, P. F.; Briant, T.; Pinard, M.; Heidmann, A. Radiation-pressure cooling and optomechanical instability of a micromirror. *Nature* **2006**, *444* (7115), 71−74.
(14) Bahl, G.; Tomes, M.; Marquardt, F.; Carmon, T. Observation of spontaneous Brillouin cooling. *Nat. Phys.* **2012**, *8* (3), 203−207.
(15) Kharel, P.; Harris, G. I.; Kittlaus, E. A.; Renninger, W. H.; Otterstrom, N. T.; Harris, J. G. E.; Rakich, P. T. High-frequency cavity optomechanics using bulk acoustic phonons. *Sci. Adv.* **2019**, *5* (4), No. eaav0582.
(16) Dykman, M. I. Heating and cooling of local and quasilocal vibration by a nonresonance field. *Sov. Phys. Solid State* **1978**, *20*, 1306−1311.
(17) Javanainen, J. Light-pressure cooling of a crystal. *Phys. Rev. Lett.* **1986**, *56* (17), 1798−1801.
(18) Zhang, J.; Zhang, Q.; Wang, X. Z.; Kwek, L. C.; Xiong, Q. H. Resolved-sideband Raman cooling of an optical phonon in semiconductor materials. *Nat. Photonics* **2016**, *10* (9), 600−605.
(19) Chen, Y. C.; Bahl, G. Raman cooling of solids through photonic density of states engineering. *Optica* **2015**, *2* (10), 893−899.
(20) Bahl, G. Raman cooling in a semiconductor. *Nat. Photonics* **2016**, *10* (9), 566−567.
(21) Khurgin, J. B. Feasibility of resonant Raman cooling and radiation balanced lasing in semiconductors. *J. Opt. Soc. Am. B* **2022**, *39* (1), 338−344.
(22) Hill, H. M.; Rigosi, A. F.; Roquelet, C.; Chernikov, A.; Berkelbach, T. C.; Reichman, D. R.; Hybertsen, M. S.; Brus, L. E.; Heinz, T. F. Observation of Excitonic Rydberg States in Monolayer MoS_2 and WS_2 by Photoluminescence Excitation Spectroscopy. *Nano Lett.* **2015**, *15* (5), 2992−2997.
(23) Lai, J. M.; Xie, Y. R.; Zhang, J. Detection of electron-phonon coupling in two-dimensional materials by light scattering. *Nano Res.* **2021**, *14* (6), 1711−1733.
(24) Barton, R. A.; Storch, I. R.; Adiga, V. P.; Sakakibara, R.; Cipriany, B. R.; Ilic, B.; Wang, S. P.; Ong, P.; McEuen, P. L.; Parpia, J. M.; Craighead, H. G. Photothermal Self-Oscillation and Laser Cooling of Graphene Optomechanical Systems. *Nano Lett.* **2012**, *12* (9), 4681−4686.
(25) Xie, H.; Jiang, S.; Rhodes, D. A.; Hone, J. C.; Shan, J.; Mak, K. F. Tunable Exciton-Optomechanical Coupling in Suspended Monolayer $MoSe_2$. *Nano Lett.* **2021**, *21* (6), 2538−2543.
(26) Liu, C.-H.; Kim, I. S.; Lauhon, L. J. Optical Control of Mechanical Mode-Coupling within a MoS_2 Resonator in the Strong-Coupling Regime. *Nano Lett.* **2015**, *15* (10), 6727−6731.
(27) Morell, N.; Reserbat-Plantey, A.; Tsioutsios, I.; Schädler, K. G.; Dubin, F.; Koppens, F. H. L.; Bachtold, A. High Quality Factor Mechanical Resonators Based on WSe_2 Monolayers. *Nano Lett.* **2016**, *16* (8), 5102−5108.
(28) Zhang, N.; Surrente, A.; Baranowski, M.; Maude, D. K.; Gant, P.; Castellanos-Gomez, A.; Plochocka, P. Moiré Intralayer Excitons in a $MoSe_2/MoS_2$ Heterostructure. *Nano Lett.* **2018**, *18* (12), 7651−7657.
(29) Lin, M. L.; Tan, Q. H.; Wu, J. B.; Chen, X. S.; Wang, J. H.; Pan, Y. H.; Zhang, X.; Cong, X.; Zhang, J.; Ji, W.; Hu, P. A.; Liu, K. H.; Tan, P. H. Moire Phonons in Twisted Bilayer MoS_2. *ACS Nano* **2018**, *12* (8), 8770−8780.
(30) Tan, Q. H.; Sun, Y. J.; Liu, X. L.; Zhao, Y. Y.; Xiong, Q. H.; Tan, P. H.; Zhang, J. Observation of forbidden phonons, Fano resonance and dark excitons by resonance Raman scattering in few-layer WS_2. *2D Mater.* **2017**, *4* (3), 031007.
(31) Lin, M. L.; Zhou, Y.; Wu, J. B.; Cong, X.; Liu, X. L.; Zhang, J.; Li, H.; Yao, W.; Tan, P. H. Cross-dimensional electron-phonon coupling in van der Waals heterostructures. *Nat. Commun.* **2019**, *10* (1), 2419.
(32) Lebedew, P. Untersuchungen über die Druckkräfte des Lichtes. *Annalen der Physik* **1901**, *311* (11), 433−458.
(33) Rand, S. C. Raman laser cooling of solids. *J. Lumin.* **2013**, *133* (0), 10−14.
(34) Aspelmeyer, M.; Kippenberg, T. J.; Marquardt, F. Cavity optomechanics. *Rev. Mod. Phys.* **2014**, *86* (4), 1391−1452.
(35) Cleland, A. Photons refrigerating phonons. *Nat. Phys.* **2009**, *5* (7), 458−460.
(36) Li, Y. L.; Chernikov, A.; Zhang, X.; Rigosi, A.; Hill, H. M.; van der Zande, A. M.; Chenet, D. A.; Shih, E. M.; Hone, J.; Heinz, T. F. Measurement of the optical dielectric function of monolayer transition-metal dichalcogenides: MoS_2, $MoSe_2$, WS_2, and WSe_2. *Phys. Rev. B* **2014**, *90* (20), 205422.
(37) Li, X. L.; Qiao, X. F.; Han, W. P.; Zhang, X.; Tan, Q. H.; Chen, T.; Tan, P. H. Determining layer number of two-dimensional flakes of transition-metal dichalcogenides by the Raman intensity from substrates. *Nanotechnology* **2016**, *27* (14), 145704.
(38) Carvalho, B. R.; Malard, L. M.; Alves, J. M.; Fantini, C.; Pimenta, M. A. Symmetry-dependent exciton-phonon coupling in 2D and bulk MoS_2 observed by resonance Raman scattering. *Phys. Rev. Lett.* **2015**, *114* (13), 136403.
(39) Varshni, Y. P. Temperature dependence of the energy gap in semiconductors. *Physica* **1967**, *34* (1), 149−154.
(40) Tan, Q. H.; Ren, S. L.; Shen, T.; Liu, X. L.; Shi, W.; Sun, Y. J.; Deng, H. X.; Tan, P. H.; Zhang, J. Unraveling the Defect Emission and Exciton-Lattice Interaction in Bilayer WS_2. *J. Phys. Chem. C* **2019**, *123* (7), 4433−4440.
(41) Gigan, S.; Bohm, H. R.; Paternostro, M.; Blaser, F.; Langer, G.; Hertzberg, J. B.; Schwab, K. C.; Bauerle, D.; Aspelmeyer, M.; Zeilinger, A. Self-cooling of a micromirror by radiation pressure. *Nature* **2006**, *444* (7115), 67−70.

https://doi.org/10.1021/acs.nanolett.2c02240
Nano Lett. 2022, 22, 7129−7135